PAPER • OPEN ACCESS

Computing the flow past Vortex Generators: Comparison between RANS Simulations and Experiments

To cite this article: M Manolesos *et al* 2016 *J. Phys.: Conf. Ser.* **753** 022014

View the article online for updates and enhancements.

Computing the flow past Vortex Generators: Comparison between RANS Simulations and Experiments

M Manolesos[1, 4], N N Sørensen[2], N Troldborg[2], L Florentie[3], G Papadakis[1], S Voutsinas[1]

[1]Laboratory of Aerodynamics, National Technical University of Athens
9 Heroon Polytechneiou Str., 15780 Athens, Greece
[2]Technical University of Denmark, DTU Wind Energy, Risø Campus,
Frederiksborgvej 399, 4000 Roskilde, Denmark
[3]Delft Technical University, Faculty of Aerospace Engineering,
Kluyverweg 1, 2629 HS, Delft, The Netherlands
[4]Flowfield Private Company, Antigonis 6, Athens, Greece

Email: marinos@fluid.mech.ntua.gr

Abstract. The flow around a wind turbine airfoil equipped with Vortex Generators (VGs) is examined. Predictions from three different Reynolds Averaged Navier Stokes (RANS) solvers with two different turbulence models and two different VG modelling approaches are compared between them and with experimental data. The best results are obtained with the more expensive fully resolved VG approach. The cost efficient BAY model can also provide acceptable results, if grid related numerical diffusion is minimized and only force coefficient polars are considered.

1. Introduction

Passive Vortex Generators (VGs) are small vanes that protrude a wing surface close to its leading edge and generate streamwise vortices that delay flow separation by bringing high momentum fluid close to the wing surface, thus energizing the local boundary layer (BL).

VGs are already being used on wind turbine blades and the ability to predict their performance is crucial as it could permit an improved blade design. The main challenge in computing the flow past VGs comes from their small size, as their height is at the order of the local BL, i.e. orders of magnitude smaller than the local blade chord, let alone the rotor diameter. A different challenge is the highly vortical 3D flow that can be an issue for Reynolds Averaged Navier Stokes (RANS) simulations utilizing eddy viscosity models.

The present study examines different numerical approaches to the issue of predicting the flow past VGs and compares them to experimental data in view of defining some "best practice" guidelines with respect to RANS computation of the flow around airfoils equipped with VGs. Simulations were performed using three different codes with two different turbulence models using different approaches with regard to VG modelling so that a variety of intercomparisons can be made.

The next two sections give the experimental and numerical details of the study. In section 4 the results are presented and discussed while the paper closes with concluding remarks given in the final section.

2. Experimental Details

The experimental data are taken from [1, 2] where the flow over a wind turbine airfoil with and without VGs was examined using pressure and Stereo Particle Image Velocimetry (PIV) measurements. Force coefficient polars and pressure distributions are available at Re = 0.87e6 for the 18% thick airfoil.

The flow velocity field was measured using Stereo PIV at $\alpha = 10°$ on three planes normal to the free stream at X/c = 0.6 (Plane A), 0.7 (Plane B), and 0.8 (Plane C). Figure 1 shows all planes with respect to both the global (X/c) and local (Δx/h) coordinates. The interrogation area for the PIV data was 16px or 0.8mm while the minimum resolved velocity for a pulse separation time of 12 μsec was U_{res} = 0.4m/s, see Table 1. Any estimated velocity lower than U_{res} is not reliable [1]. All data are normalized with U_∞ and the chord length (c = 0.6m), unless otherwise specified.

Table 1. Stereo PIV test details for all the planes measured

	Plane A	Plane B	Plane C
Chordwise location (X/c)	0.6	0.7	0.8
Distance from VG trailing edge (Δx/h)	27.2	37.2	47.2
Final interrogation area size [px]		16	
Final interrogation area size [mm]		0.8	
Minimum resolvable velocity [m/s]		0.4	
Minimum resolvable velocity [normalized with respect to the free stream velocity]		2%	
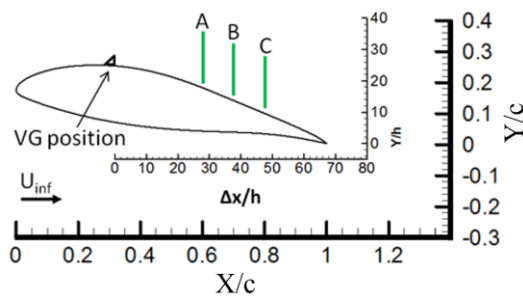
Figure 1. Stereo PIV measurement planes given in global (X/c) and local (Δx/h) coordinates. In global coordinates the chordwise axis starts at the airfoil LE, while in local coordinates it starts at the VG TE.
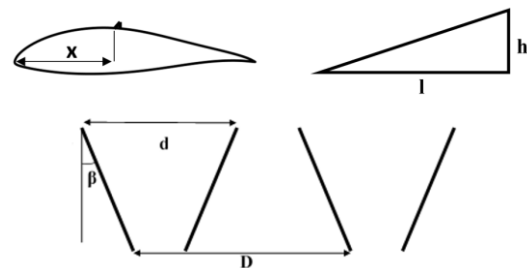
Figure 2. Triangular vane vortex generator parameters. Top left: Airfoil side view, Top right: VG side view, Bottom VG top view.

Triangular VGs were used in this investigation, as shown in Figure 2. The VG height was equal to the local BL thickness, which was δ = 6mm, based on RANS simulations. The VGs upstream of the measurement planes were always met with turbulent flow as a 0.4mm high ZZ tape was used as a stabilizing mechanism for Stall Cells that appear at higher angles of attack [3]. The details of the selected configuration are given below:

X	=	0.3c	chordwise position of the VG array
β	=	20°	VG angle to the free stream flow
h	=	δ = 6mm	VG height
l	=	3h	VG length
D	=	11.7h	distance between two VG pairs
d	=	3.7h	spanwise distance between the LE of two VGs of the same pair

In the experiments the VGs were constructed using a 0.2mm thick aluminium strip that was positioned

on the wing suction surface. This is a common technique [4-6] that ensures adequate rigidity for the VGs, while imposing minimum disturbance to the BL.

A short note regarding near and post stall behaviour is required prior to comparing the numerical results with the experimental data. In the experiments, Stall Cells (SCs) develop on the suction side of the airfoil at angles of attack near and after stall, a typical behaviour for airfoils exhibiting TE separation [7]. It has been shown [8] that simulations of very limited width like the ones presented here cannot predict the onset of SCs due to the limited spanwise extent of the computational domain. So, the reader should bear in mind that at higher angles of attack the actual 3D separation phenomenon observed in the experiments is not captured by the limited width simulations presented in this study, even if force coefficients or Cp values between the simulations and the experiments are similar.

The pressure taps were located at the centre of the wing model, so the experimental pressure distributions and force coefficient values refer to the state of the flow at the centre of the wing span, which was also the centre of the SC [3]. This means that the wing section where the separation line is at its most upstream position is examined. SCs on the present airfoil appear for $\alpha > 6°$ for the clean case and for $\alpha > 11°$ for the case with VGs.

Finally, it is noted that modern multi MW wind turbines operate Re numbers almost an order of magnitude larger than the Re number in this study. However, to the best of our knowledge no VG experiments at Re numbers of O(10e6) are available, so the validation of the numerical tools had to be performed against the available experimental data.

3. Numerical Details
In this section the three different RANS solvers are shortly presented along with the two different modelling approaches with respect to VG treatment.

3.1. Solvers and Vortex Generator modelling

3.1.1 EllipSys3D
EllipSys3D is an in-house incompressible finite volume Reynolds Averaged Navier - Stokes solver developed at DTU [9]. The computations were performed in steady state and the kω SST turbulence model [10] was used.

Two approaches were followed with regards to VG treatment. In the more detailed and expensive one the VG geometry was fully resolved in the computational mesh (see Figure 4), while in the other a variation of the BAY [11] model is used.

The fully resolved (FR) VG modelling is not to be considered as a separate model, but a special set-up procedure mainly relying on the grid generation. In order to limit the computational requirements, the geometrical symmetry of the VG's is exploited by only resolving one of the two vanes in a VG pair while symmetry conditions are used on the sides of the simulated area as sketched in Figure 3.
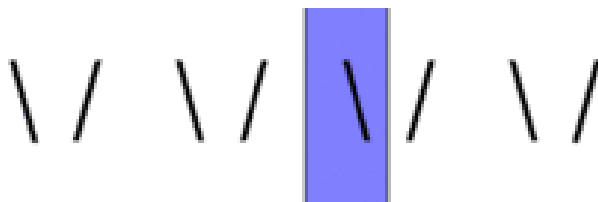
Figure 3. Top view of a VG array. VG symmetry was exploited and the flow was simulated only inside the highlighted area with symmetry conditions at the side boundaries.

The BAY model assumes that the presence of a zero thickness vane VG can be represented as a source term in the momentum and energy equations. This term simulates the force introduced by the VG in the flowfield and aligns the flow with the VG direction. Details about the implementation can be found in [12]. Two pairs of VGs were considered in the BAY simulations with symmetry conditions at the side boundaries.

In the remaining of this text the two EllipSys simulations will be referred to as EllipSys – FR – kω and EllipSys – BAY – kω, for the Fully Resolved and the BAY model approach, respectively.

Figure 4. An example of a meshed VG unit from the EllipSys – FR – kω simulations. The left picture shows the VG surface with the block structure around the VG and the right picture shows the surface grid on the VG unit. Every other grid line is shown for clarity.

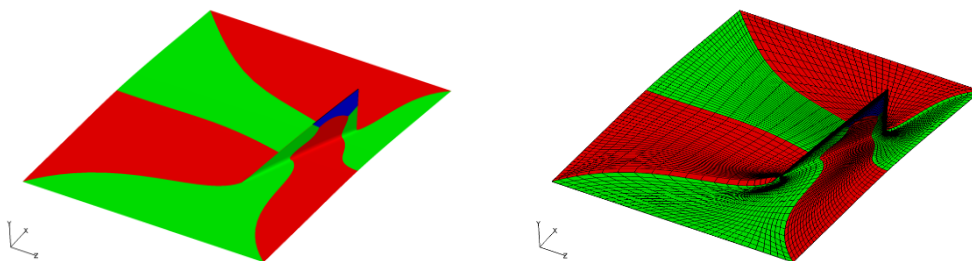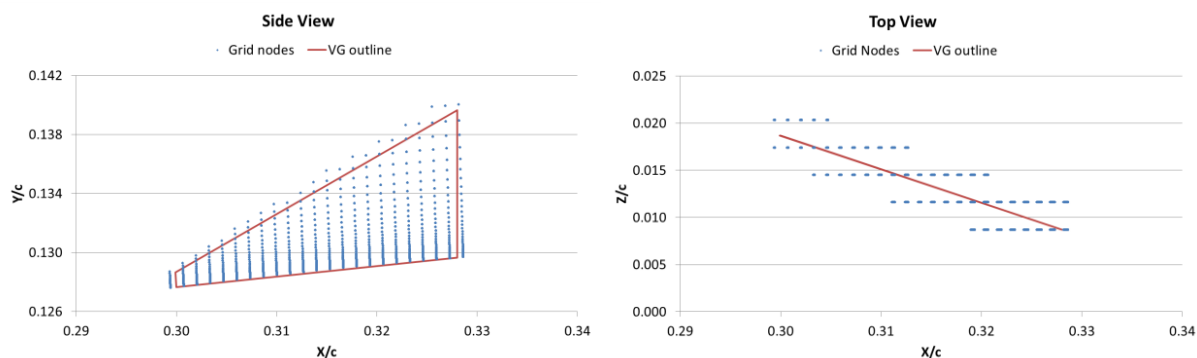**Figure 5.**: VG outline and grid nodes of the cells where the BAY model is applied for the MaPFlow computations. Side view (left) and Top view (right).

3.1.2   MaPFlow

MaPFlow is a multi-block MPI enabled compressible solver equipped with preconditioning in regions of low Mach flow, developed at NTUA [13]. The solver is equipped with the Spalart-Allmaras (SA) [14] and the kω SST eddy viscosity turbulence models, both of which were used in the current investigation.

The effect of the VGs on the flow is included by means of the BAY model. The model was applied in its jBAY variation [15] in which the VG is replaced by a surface with zero thickness. The cells to which the source term is added, are the cells that intersect this VG surface, see Figure 5.

The two MaPFlow simulations will be referred to as MaPFlow – BAY – kω and MaPFlow – BAY – SA, to distinguish between the two different turbulence models used. All SA simulations were steady state. Simulations with the kω model for the clean airfoil case were steady for $\alpha < 10°$ and unsteady for higher angles of attack with dt = 0.001. For the case with VGs the only unsteady simulations were at 14° and 15° with dt = 0.005.

3.1.3   OpenFOAM

OpenFOAM is an open-source software for computational fluid dynamics distributed under the General Public Licence, thereby giving users the freedom to modify the source code and develop their own additional modules. It is a segregated finite volume code able to solve compressible and incompressible flows on either structured or unstructured grids. For the current work, the steady, incompressible RANS equations are solved using the kω SST turbulence model.

Similar to EllipSys3D and MaPFlow, the effect of VGs is accounted for using the BAY model. A source term that corresponds to the side force imposed on the flow by the VG is locally added to the momentum equation. The cells where this source term is applied are chosen so as to correspond to the physical location of the VG, using the same zero thickness approach as described in section 3. The OpenFOAM simulation will be referred to as **OpenFOAM – BAY – kω** in the remaining of the text.

3.2. Computational Mesh

In each of the computations a different numerical grid was used except for the MaPFlow computations which shared the same mesh. Details on all grids are given in Table 2.

For the fully resolved case (EllipSys – FR – kω) a parametric multi-process grid generation strategy was followed that limits the necessary effort to generate the mesh [12]. The main parameters of interest in this procedure are the chord-wise position of the VGs, VG size, VG aspect ratio, VG inclination and the inter and intra spacing of the VG pairs. An example is given in Figure 4.

For the MaPFlow cases a 2D structured grid was initially created with local refinement around the VG region and up to 2h from the wing surface in the normal direction. A similar procedure was followed in the EllipSys – BAY – kω simulations, although without the local refinement around the VG area. For the OpenFOAM simulations a structured mesh was created by first generating a 2D C-mesh close to the surface of the airfoil, and surrounding it by an O-mesh. Local mesh refinement in the chordwise direction was applied near the leading edge, trailing edge and in the vicinity of the VG location. In all BAY model simulations, the grid was extruded in the spanwise direction in different number of equal steps, see Table 2.

It is noted that in the EllipSys – BAY – kω case, a total number of four VGs were considered, while only one VG was simulated in all other computations. Thus, this was the coarsest grid of the present study, with MaPFlow and OpenFOAM grids having 5.0 and 15.0 times more cells. In terms of total number of cells, the EllipSys – FR – kω grid was in fact smaller than the largest BAY model grid (OpenFOAM) and had 11.8 times more cells than the coarsest mesh (EllipSys – BAY).

Table 2. Computational mesh details for each simulation

Simulation	EllipSys – FR – kω	EllipSys – BAY – kω	MaPFlow – BAY (kω and SA)	OpenFOAM – BAY – kω
VG Chordwise resolution	128	3	22	28
VG Normal resolution	64	58	45	46
VG Spanwise resolution	64	2	4	11
Mesh Type	O-type	O-type	C-type	mixed
Chordwise resolution	384	256	468	424
Normal resolution	128	128	135	139
Spanwise resolution	64	32	20	59
Y+	<2	<2	<1	<1
Number of VGs considered	1	4	1	1
Width of the computational domain	0.058c	0.232c	0.058c	0.058c
Far-field boundary	30c	30c	50c	50c
Total number of cells [millions]	3.1	1.05	1.3	4.0
Number of cells per VG [millions]	3.1	0.26	1.3	4.0

4. Results and discussion

4.1. Clean Airfoil

There is good agreement in the linear part of the force coefficient polars between the experiments and all simulations (see Figure 6). At higher angles of attack all simulations overpredict Cl, as expected, since they cannot predict 3D separation (see [2, 16]). Over the same range of angles of attack, Cd is underpredicted compared to the measured data, with OpenFOAM giving the lowest drag values among the kω computations.

   With regard to the agreement between the different simulations, EllipSys, OpenFOAM (incompressible codes) and MaPFlow (compressible code) predict very similar results with the kω model, despite the very low Ma number (~0.01). On the contrary, MaPFlow results with the SA turbulence model show delayed onset of separation and higher Cl_{max} values compared to the relevant kω simulations. In Figure 7, the skin friction coefficient (Cf) distribution at α = 10° for the two MaPFlow simulations confirms that in the kω case the separated region is larger and Cf is lower around the airfoil indicating that the BL is thicker and more prone to separation.
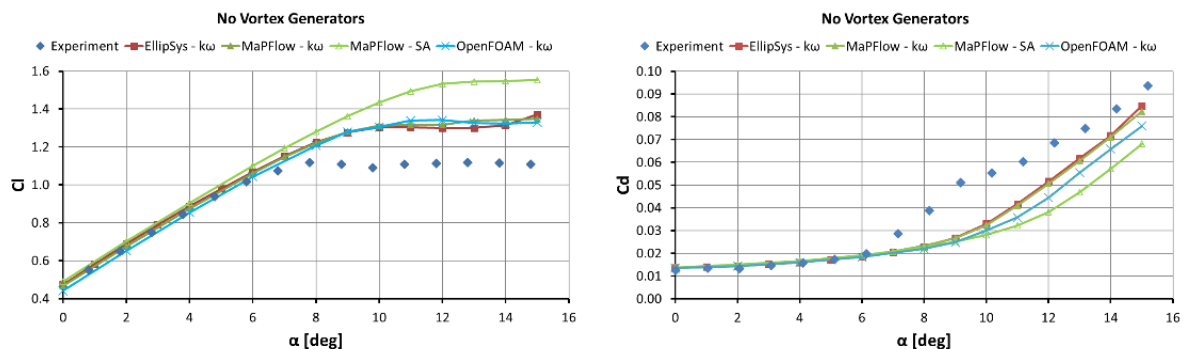

Figure 6. Lift (left) and drag (right) polars for the case without VGs.
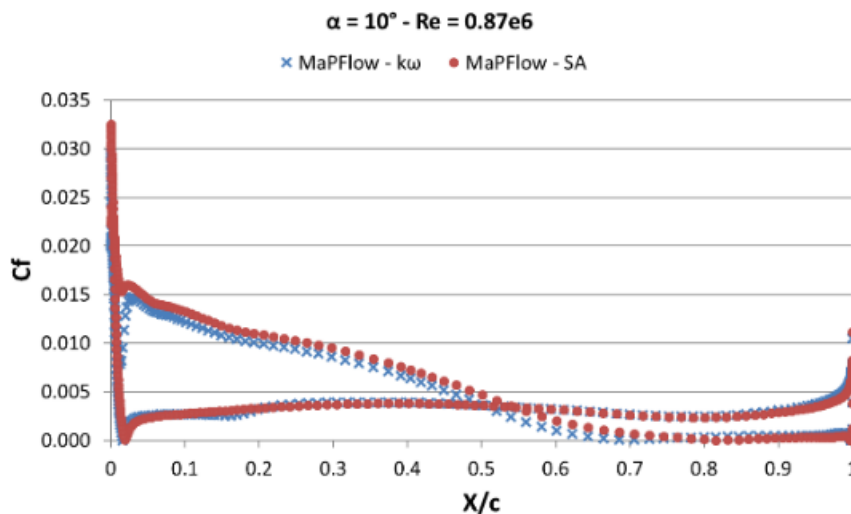
Figure 7. Friction coefficient distribution along the airfoil for the case without VGs. MaPFlow simulations with the kω and SA turbulence models are compared. Lower Cf values and larger separation are predicted by the kω model.

4.2. Airfoil with Vortex Generators

For the case with VGs, the Cl predictions agree well between them in the linear part of the Cl and Cd polars, see Figure 8. Compared to the experiments, dCl/dα and lift are overpredicted, the latter especially at higher AoA, while the drag increase due to the VGs is underpredicted. At higher angles of attack all codes underpredict drag coefficient values except the EllipSys – BAY – kω which gives slightly higher drag values. The lowest drag values are predicted by the OpenFOAM – BAY – kω simulation.

It is possible that the difference in VG drag penalty at lower angles of attack between predictions and measurements is partially due to the fitting of the VGs on the wind tunnel model. The aluminium strip used, despite its very small thickness, is expected to cause a thicker BL and hence higher drag and reduced lift gradient, an effect not accounted for in the simulations.

Figure 8. Lift (left) and drag (right) polars for the case with VGs.

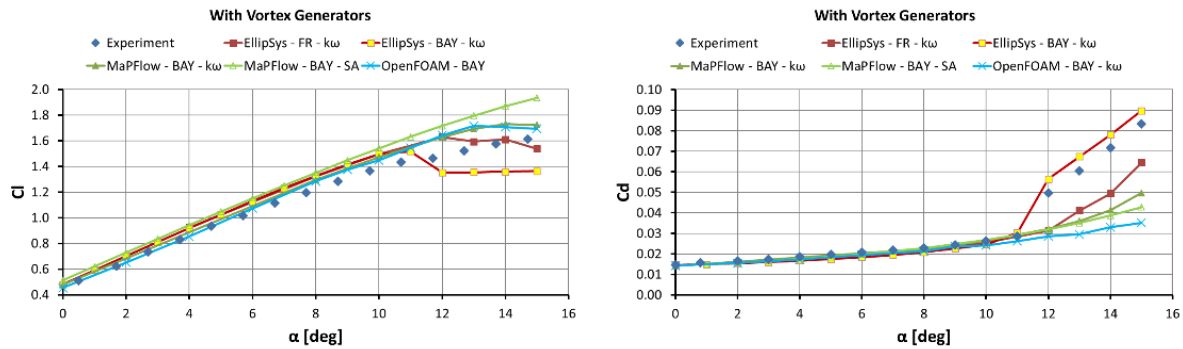Part of the difference in Cl values is attributed to the limited spatial resolution in the measurements. As Figure 9 shows for $\alpha = 10°$, the agreement between experiments and predictions is very good, with the main differences appearing close to the wing LE. The limited number of pressure taps in the LE region as well as the fact that they extend only up to 88.8% chord is partially responsible for the difference in Cl values.
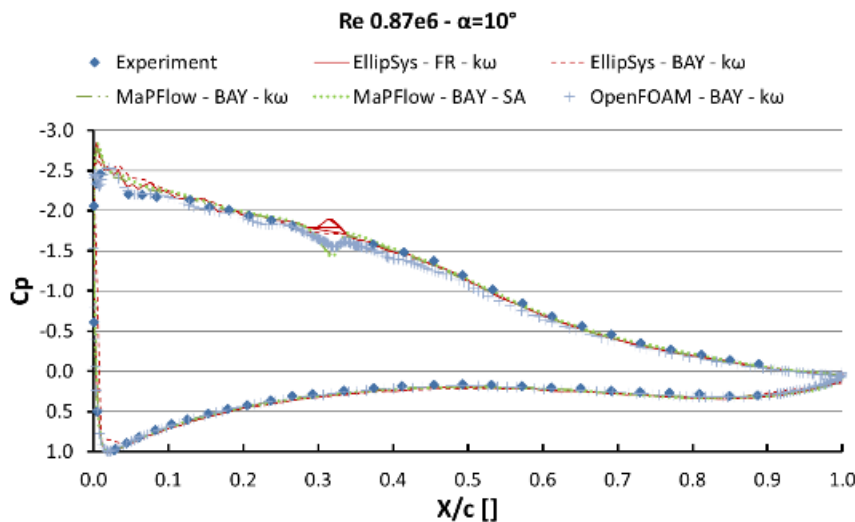

Figure 9. Pressure coefficient distribution around the airfoil. Data from experiments and simulations. Measurements in the vicinity of the VG and the ZZ tape are not shown for clarity.

In the experiments a small SC is formed at 12° that significantly reduces the $dCl/d\alpha$ gradient beyond that point, which, however, remains positive with Cl_{max} appearing at $\alpha_{Clmax} = 15°$. In the computations, only MaPFlow – BAY – SA correctly predicts α_{Clmax}, albeit with overpredicted Cl values. OpenFOAM – BAY – kω and MaPFlow – BAY – kω lift data are very similar, with OpenFOAM predicting lower Cd values. EllipSys – FR – kω and EllipSys – BAY – kω predict maximum lift at lower angles of attack, at 12° and 11°, respectively. With regard to the turbulence model effect, predicts lower Cl_{max} and earlier separation compared to the SA results, as observed by the comparison of the two MaPFlow simulations. This behaviour is consistent with the observations from the clean airfoil case.

VG effectiveness is expected to be greater when the vortex is stronger, i.e. in the EllipSys – FR – kω case. The fact that contrary to this, there is a drop in the lift polar from the specific simulation is linked to grid imperfections close to the airfoil LE and not to the vortex strength. The numerical mesh used was based on noisy geometry measurements form the actual wing model used in the experiments. These

imperfections lead to pressure fluctuations visible in in Figure 9 and possibly to earlier onset of stall at higher angles of attack.

By comparing the two EllipSys simulations it can be deduced that the vortex generated in the BAY model computation is less effective in energizing the decelerating BL and thus stall appears at a lower angle of attack. As shown in section 4.1, the vortex is more diffused in the BAY simulations not only due to the way it was created, but also due to excessive numerical diffusion linked to insufficient grid resolution.

4.2.1 Flow field at 10° - Comparison with the experimental results

In this section a closer look is taken at the flowfield downstream of the VGs comparing the numerical predictions with Stereo PIV data.

Figure 10 and Figure 11 show the streamwise velocity and vorticity contours, respectively, on planes A, B and C from all sets of data. In the first column, Stereo PIV measurements are plotted on the left half of each image while on the right half numerical data from EllipSys – FR – kω are given. In the central column, each image shows data from the from EllipSys – BAY – kω (left) and OpenFOAM – BAY – kω (right) simulations. The relevant data from the two MaPFlow – BAY simulations are given in the third column, with SA and kω results presented on the left and right half of the images, respectively.

In the aforementioned figures the scale is always the same and the wing surface is at Y/h=0. On all plots vorticity isolines of $\omega_{0.5} = \omega_{max}/2$ (ω_{max} is the peak vorticity on each plane) are drawn to indicate the location and size of the vortex core. A streamwise velocity isoline is also drawn, indicating the BL height at the sides of the VG pair. The specific value, U_{BL}, corresponds to the U value at the height where $\partial U / \partial y \approx 0$, at z/h = ±5.8. In order to highlight the differences in grid resolution between the various sets of data, in the last row of Figure 11 (plane C), the grid lines are superimposed on the vorticity contours.

It is noted at this point that since vorticity is a quantity that is strongly dependent on grid topology and density, it should not be compared quantitatively between cases with different mesh. Still, the general trends can be safely juxtaposed.

All simulations capture qualitatively the distinct Ω shape of the BL and vortex diffusion from plane A to plane C. The working principle of the VGs is also well demonstrated as high momentum fluid is brought towards the wing surface at the sides of the vortices and low momentum fluid is raised in the region between them by their combined upwash. In terms of velocity contours, the low velocity region between the two vortices is best captured in the coarse simulations.

In the vorticity contours the VG vortex is clearly distinguished within the Ω region, i.e. embedded in the BL. The highest vorticity values are observed in the EllipSys – FR – kω and the OpenFOAM – BAY – kω results. This suggests that numerical diffusion is at least as critical as the vortex formation mechanism in this case. The vortex shape is best captured by the EllipSys – FR – kω simulation, while two vorticity peaks appear in the BAY simulation results. Two vorticity peaks appear also on the experimental data on plane B (Figure 11). It is currently unclear whether this double peak is an artefact linked to grid resolution or it is a genuine phenomenon.

In the coarser BAY model simulations (MaPFlow and EllipSys), the vortex is more diffused and $\omega_{0.5}$ is smaller, with significantly lower vorticity values observed in the EllipSys – BAY – kω case, as expected due to the limited spanwise resolution of the numerical grid used. This partially justifies the fact that EllipSys – BAY – kω predicts lower Cl_{max} and α_{Clmax} values (see Figure 8). As vortex diffusion is overpredicted, vortex effectiveness in separation control is underestimated.

4.2.2 Effects of the applied turbulence modelling

In this section results from the two MaPFlow – BAY computations are compared to examine the effect of the applied turbulence modelling. While it is accepted [17-19] that eddy viscosity models tend to overpredict vortex diffusion and vortex strength decay, it is still important to understand what the differences between the two models are, since both models are widely used in both the academic and the industrial sector.
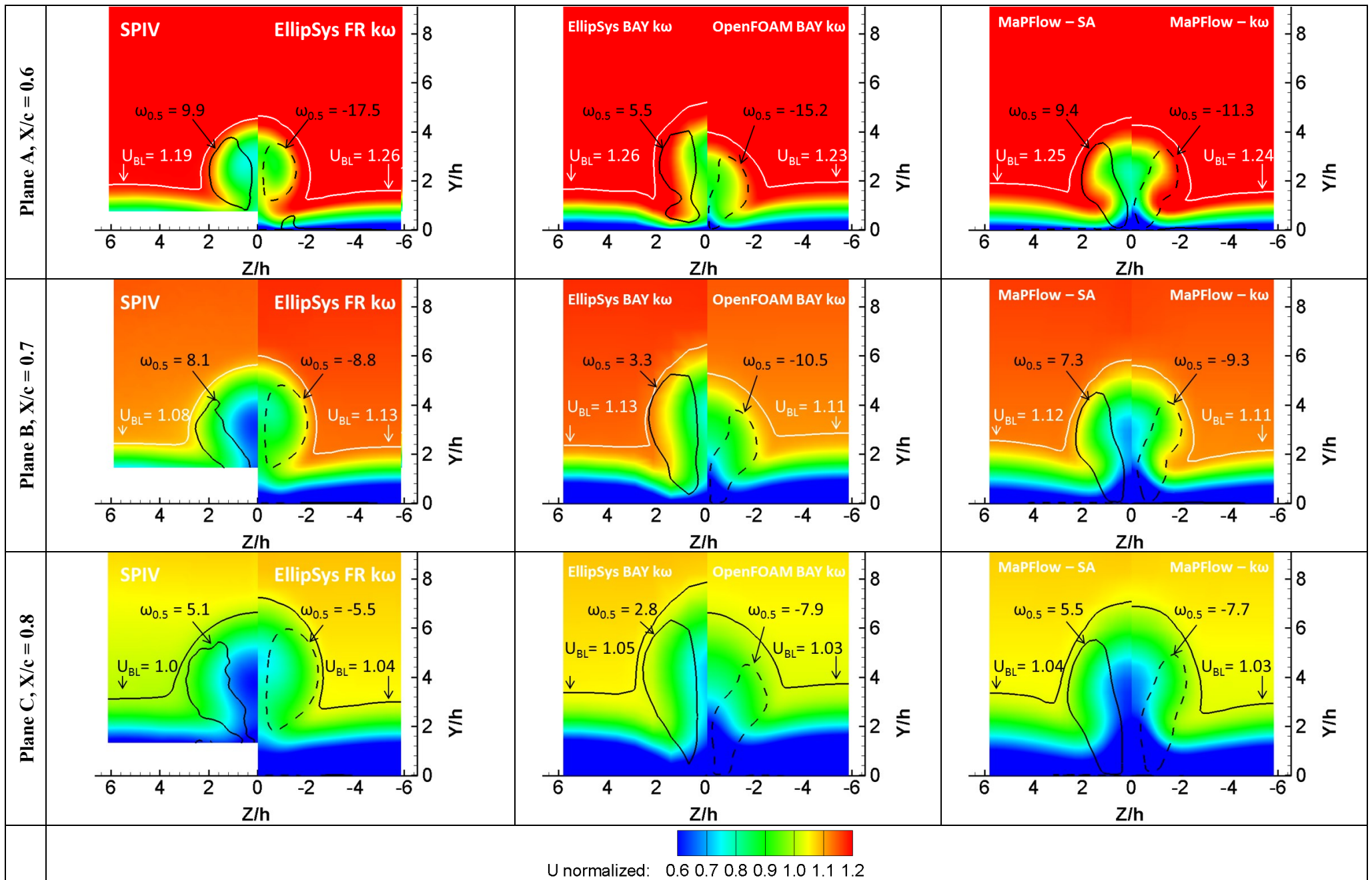
Figure 10. Streamwise velocity contours on planes A, B and C. Results from experiments and all simulations.
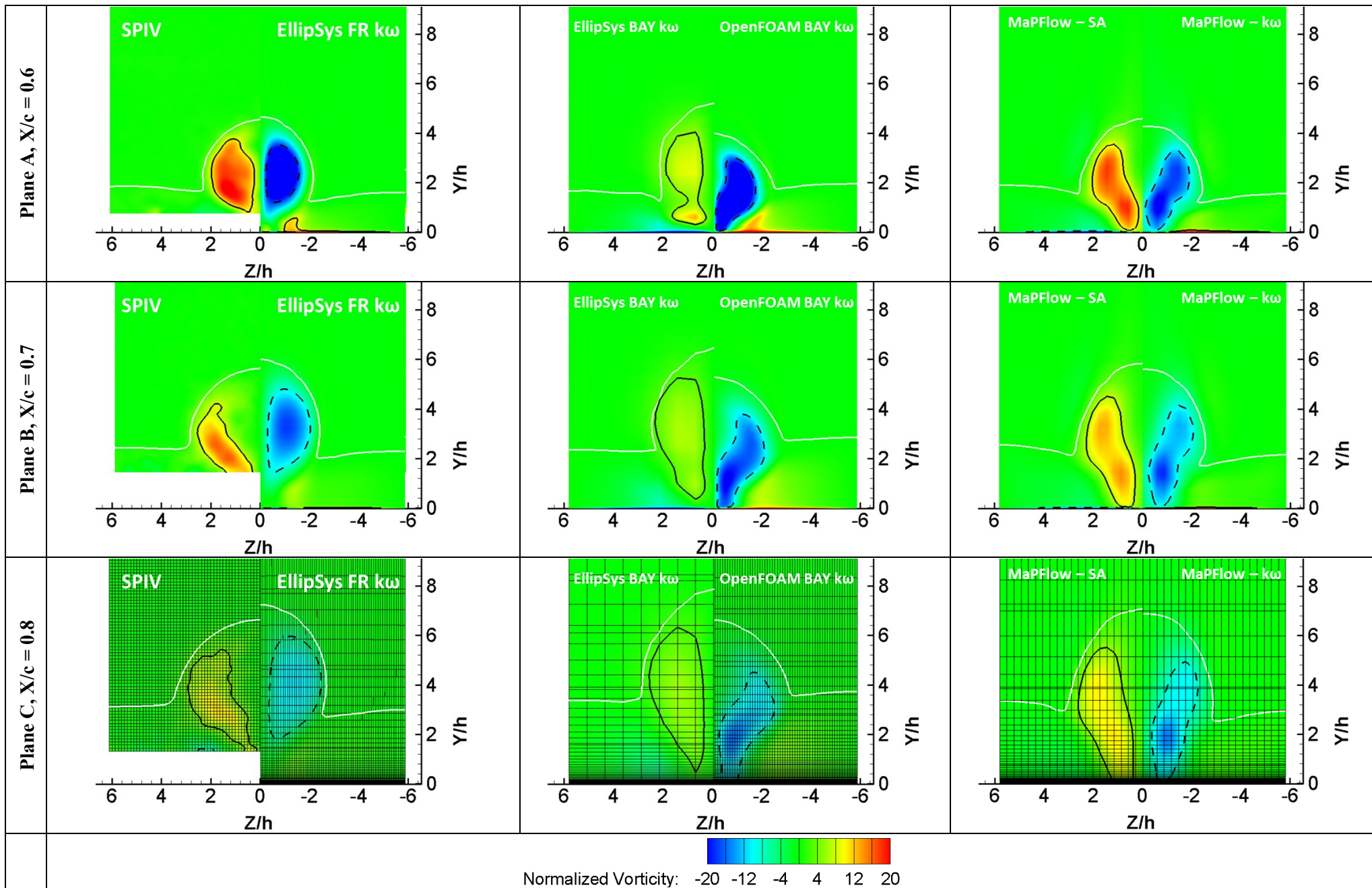
Figure 11. Streamwise vorticity contours on planes A, B and C. Results from experiments and all simulations. Grid lines are superimposed on the contours of plane C

The vortex in the kω simulations is less diffused and peak vorticity drops at a lower rate compared to the SA computation, as shown in Figure 10 and Figure 11. The shape of the vortex is very similar for both models suggesting that in the present case it is dominated by the grid resolution rather than the selection of turbulence model. Figure 12 gives the peak vorticity variation with distance from the VG TE for the two cases which were run on the same grid.

In comparison to the SA model, the kω model appears to produce two counteracting effects, one that leads to increased effectiveness in separation control (less diffused VG vortex) and one that leads to earlier separation (BL more prone to separation). The combined result is the earlier separation and lower Cl_{max} predicted in the MaPFlow – BAY – kω simulations.
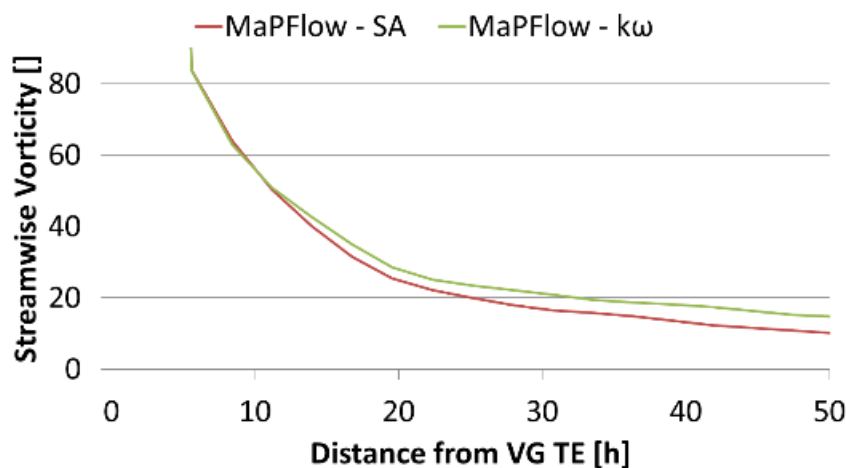

Figure 12. Absolut peak vorticity variation with distance from the VG TE. Results from the SA and kω MaPFlow simulations performed on the same grid.

5. Conclusions

Numerical predictions from three different RANS solvers using two different turbulence models and two different VG modelling approaches were compared with experimental measurements. The comparisons concerned force coefficient polars and flow field data, like velocity and vorticity.

Good agreement is found between predictions and experiments in the linear part of the polar, i.e. as long as the flow remains attached and two dimensional. As expected, when 3D separation occurs the agreement deteriorates as the low aspect ratio simulations examined in this study are not able to capture the Stall Cell phenomenon. The VG drag penalty is underpredicted by all simulations, possibly due to the way the VGs were added on the wind tunnel model.

In terms of VG modelling, the fully resolved simulation shows the best agreement with the experimental data in terms of vortex shape and the latter appears to be strongly dependent on grid resolution, especially for the BAY model results. Predictions using the BAY model compare favourably to the fully resolved simulations in terms of force coefficients at lower AoA. It is noted that although BAY model simulations have significantly reduced meshing requirements compared to the FR case, local refinement around the VG is still important in order to reduce numerical diffusion.

The agreement between the three codes when the same turbulence model is used is very good for the clean airfoil case, while grid differences are believed to cause the discrepancy at higher AoA for the case with VGs.

In comparison to the SA model, the kω SST model appears to produce two counteracting effects, one that leads to increased effectiveness in separation control (less diffused VG vortex) and one that leads to earlier separation (BL more prone to separation). The combined result is the earlier separation and lower Cl_{max} predicted in the kω simulations.

The overall conclusions can be summarized as follows. The more expensive fully resolved approach provides the best results. However, if details of the flowfield downstream of the VGs are not required and only lift and drag coefficient polars are of interest, then a sufficiently resolved BAY simulation can provide acceptable results. In any case, agreement with experiments is only expected in the linear part

of the polar, i.e. prior to Cl_{max}, as the limited width of the computational domain of the present simulations does not allow for the prediction of 3D separation.

References

[1]　Manolesos, M. and Voutsinas, S. G.　2015 "Experimental investigation of the flow past passive vortex generators on an airfoil experiencing three-dimensional separation" *Journal of Wind Engineering and Industrial Aerodynamics* Vol 142　2015 pp 130-148

[2]　Manolesos, M.Papadakis, G. and Voutsinas, S. G.　2013 "Experimental and computational analysis of stall cells on rectangular wings" *Wind Energy* Vol 17 No 6 2013　doi: 10.1002/we.1609

[3]　Manolesos, M. and Voutsinas, S. G.　2013 "Geometrical characterization of stall cells on rectangular wings" Wind Energy Vol 17 No 9 2013 pp 1301-1314 doi: 10.1002/we.1634

[4]　Fuglsang, P.Antoniou, I.Dahl, K. S. and Aagaard Madsen, H.　1998 "Wind tunnel tests of the FFA-W3-241, FFA-W3-301 and NACA 63-430 airfoils. " Risø-R 1041.

[5]　Bak, C.Fuglsang, P.Johansen, J. and Antoniou, I.　2000 "Wind tunnel tests of the NACA 63-415 and a modified NACA 63-415 airfoil " Risø-R-1193.

[6]　Fuglsang, P.Bak, C.Gaunaa, M. and Antoniou, I.　2003 "Wind tunnel tests of Risø-B1-18 and Risø-B1-24. " Risø-R-1375.

[7]　Broeren, A. P. and Bragg, M. B.　1998 "Low-frequency flowfield unsteadiness during airfoil stall and the influence of stall type" AIAA Paper　No 2517 1998 pp 196-209

[8]　Manolesos, M.Papadakis, G. and Voutsinas, S. G.　2014 "Assessment of the CFD capabilities to predict aerodynamic flows in presence of VG arrays" Journal of Physics: Conference Series Vol 524 No 1 2014 p 012029

[9]　Sørensen, N. N.　1995 "General purpose flow solver applied to flow over hills " PhD Thesis. Technical University of Denmark

[10]　Menter, F. R.　1993 "Zonal two-equation k-w turbulence model for aerodynamic flows" AIAA Paper　No 1993 - 2906 1993

[11]　Bender, E. E.Anderson, B. H. and Yagle, P. J.　1999 "Vortex generator modeling for Navier-Stokes codes" ASME Paper FEDSM99-6919　1999

[12]　Ferreira, C. S.Salcedo, A. G.Baldacchino, D. and Aparicio, M.　2015 "Development of aerodynamic codes for modelling of flow devices on aerofoils and rotors" AVATAR EU Project, Report　D3.2

[13]　Papadakis, G. and Voutsinas, S. G.　2014 "In view of accelerating CFD simulations through coupling with vortex particle approximations" *Journal of Physics: Conference Series* Vol 524 2014 p 012126 doi: 10.1088/1742-6596/524/1/012126

[14]　Spalart, P. R. and Allmaras, S. R.　1992 "A one-equation turbulence model for aerodynamic flows". *AIAA Journal* 94, 1992, DOI: 10.2514/6.1992-439

[15]　Jirasek, A.　2005 "Vortex-Generator Model and Its Application to Flow Control" *Journal of Aircraft* Vol 42 No 6 2005 pp 1486-1491 doi: 10.2514/1.12220

[16]　Manolesos, M. and Voutsinas, S. G.　2014 "Study of a stall cell using stereo particle image velocimetry" *Physics of Fluids* Vol 26 No 4 2014 p 045101 doi: http://dx.doi.org/10.1063/1.4869726

[17]　Lin, J. C.　2002 "Review of research on low-profile vortex generators to control boundary-layer separation" *Progress in Aerospace Sciences* Vol 38 No 4-5 2002 pp 389-420 doi: 10.1016/s0376-0421(02)00010-6

[18]   Yao, C. S.Lin, J. C. and Brian, A. G. 2002 "Flow-Field Measurement of Device-Induced Embedded Streamwise Vortex on a Flat Plate" AIAA Paper No 3162 2002

[19]   Allan, B. G.Yao, C. S. and Lin, J. C. 2002 "Numerical simulations of vortex generator vanes and jets on a flat plate" AIAA Paper No 3160 2002